
SAM-Med3D

Haoyu Wang^{1,2*} Sizheng Guo^{1*} Jin Ye^{1*} Zhongying Deng^{1*}
 Junlong Cheng¹ Tianbin Li¹ Jianpin Chen¹ Yanzhou Su¹ Ziyang Huang^{1,2}
 Yiqing Shen¹ Bin Fu³ Shaoting Zhang¹ Junjun He^{1†} Yu Qiao^{1†}

¹Shanghai AI Laboratory

²Shanghai Jiao Tong University

³ShenZhen Key Lab of Computer Vision and Pattern Recognition,
 Shenzhen Institute of Advanced Technology, Chinese Academy of Sciences
 {yejin, hejunjun, litianbin, zhangshaoting, qiaoyu}@pjlab.org.cn

Abstract

Although the Segment Anything Model (SAM) has demonstrated impressive performance in 2D natural image segmentation, its application to 3D volumetric medical images reveals significant shortcomings, namely suboptimal performance and unstable prediction, necessitating an excessive number of prompt points to attain the desired outcomes. These issues can hardly be addressed by fine-tuning SAM on medical data because the original 2D structure of SAM neglects 3D spatial information. In this paper, we introduce SAM-Med3D, the most comprehensive study to modify SAM for 3D medical images. Our approach is characterized by its comprehensiveness in two primary aspects: firstly, by comprehensively reformulating SAM to a thorough 3D architecture trained on a comprehensively processed large-scale volumetric medical dataset; and secondly, by providing a comprehensive evaluation of its performance. Specifically, we train SAM-Med3D with over 131K 3D masks and 247 categories. Our SAM-Med3D excels at capturing 3D spatial information, exhibiting competitive performance with significantly fewer prompt points than the top-performing fine-tuned SAM in the medical domain. We then evaluate its capabilities across 15 datasets and analyze it from multiple perspectives, including anatomical structures, modalities, targets, and generalization abilities. Our approach, compared with SAM, showcases pronouncedly enhanced efficiency and broad segmentation capabilities for 3D volumetric medical images. Our code is released at <https://github.com/uni-medical/SAM-Med3D>.

1 Introduction

Medical image analysis has become an indispensable cornerstone of modern healthcare, aiding diagnosis, treatment planning, and further medical research [39, 42, 17]. One of the most significant challenges in this realm is the precise segmentation of volumetric medical images [24]. Although numerous methods have demonstrated commendable effectiveness across a spectrum of targets [25, 26, 47], prevailing segmentation techniques exhibit a tendency of specialization towards specific organs or lesions. This tendency is attributed to the inherent characteristics of volumetric medical images, such as the intricacy of 3D anatomical structures and limited volumetric medical annotations [25, 6]. Consequently, this specialism impedes the generalization ability of methods, posing tangible challenges to broader clinical applicability.

*Equal contribution.

†Corresponding author.

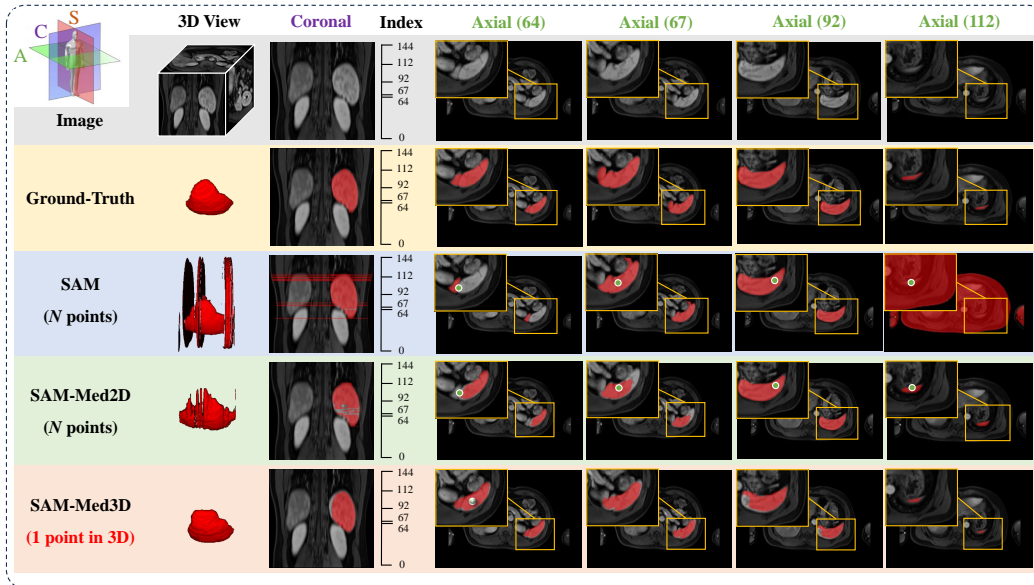


Figure 1: **Illustration of SAM [21], fine-tuned SAM (SAM-Med2D [6]), and our SAM-Med3D on 3D Volumetric Medical Images.** Both SAM and SAM-Med2D take N prompt points (one for each slice) whereas SAM-Med3D uses a single prompt point for the entire 3D volume. Here, N corresponds to the number of slices containing the target object. The top-left corner provides a schematic of the Axial, Coronal, and Sagittal views. For a given 3D input, we visualize the 3D, coronal, and multiple axial views. The numbers in brackets indicate the index of each axial slice.

Recently, the Segment Anything Model (SAM) [21], a Vision Foundation Model (VFM) trained with over 1 billion masks, has exhibited impressive zero-shot segmentation performance across numerous domains. The rise of SAM introduces new possibilities for accelerating data annotation and enhancing the methodological generalization capability for volumetric medical image analysis. Nevertheless, studies have highlighted that SAM’s native applicability to the medical domain is limited, due to the significant lack of knowledge about medical images [6, 16, 8]. A straightforward solution to infuse medical knowledge into SAM is fine-tuning with medical images. MedSAM [27] has achieved this by fine-tuning the decoder with 1.1 million masks, enabling SAM’s application in medical imaging. SAM-Med2D [6] undertakes a comprehensive adaptation by utilizing adapters and about 20 million masks, exhibiting remarkable capabilities in general medical image segmentation. However, these methods have to handle volumetric images with a slice-by-slice approach: decomposing 3D data into 2D slices, processing each slice independently, and then aggregating the 2D results into a 3D prediction. As disclosed in previous evaluation [28, 2], the slice-by-slice manner exhibits suboptimal performance on 3D medical images due to the neglect of inter-slice 3D spatial information.

Moreover, some researchers have endeavored to capture 3D spatial information via 2D to 3D adaptation [3, 11, 45]. As shown in Table 1, those methods usually freeze 2D layers but train 3D adapters to enable the model to learn from 3D images. However, these methods have two limitations: **(1) Limited data scale:** Their models are trained solely on a limited scale of data with limited types of targets. Table 1 further delineates the considerable gap between the competitors and our work in terms of both dataset size and category diversity. **(2) Inherent 2D architecture:** Their model persistently adheres to a 2D design paradigm (e.g., frozen 2D encoder), curtailing the ability to model 3D spatial information comprehensively. More details will be introduced in Section 4.

To address these limitations, we propose SAM-Med3D, a model with a fully learnable 3D architecture, and train it on a fully processed large-scale volumetric medical dataset. Our training dataset comprises 21K medical images and 131K masks with 247 categories, derived from an amalgamation of various public and private 3D medical image datasets. As evident from Figure 2, it is more than 10 times larger than the largest existing medical image segmentation datasets *TotalSegmentator* [44] and *BraTS21* [1].

Model	Dataset Size	Category	Image Encoder	Prompt Encoder	Mask Decoder
MedLSAM [23]	~ 25K masks	~ 50	❄️ 2D	❄️ 2D	❄️ 2D
SAM ^{Med} [38]	-	-	❄️ 2D	❄️ 2D	❄️ 2D
SAM3D [2]	2K masks	14	❄️ 2D	-	🔥 3D
MA-SAM [3]	5 datasets	≤ 13	❄️ 2D + 🔥 Adapter	-	🔥 2D
MSA [45]	12K masks	15	❄️ 2D + 🔥 Adapter	🔥 2D	🔥 2D
3DSAM-A [11]	≤ 1K masks	4	❄️ 2D + 🔥 Adapter	🔥 3D	🔥 3D
SAM-Med3D	131K masks	247	🔥 3D	🔥 3D	🔥 3D

Table 1: **Comparison of SAM models for 3D volumetric medical images.** Our SAM-Med3D employs a fully learnable 3D architecture with large-scale training data, instead of frozen 2D layers with adapters. ❄️ and 🔥 denotes frozen and learnable.

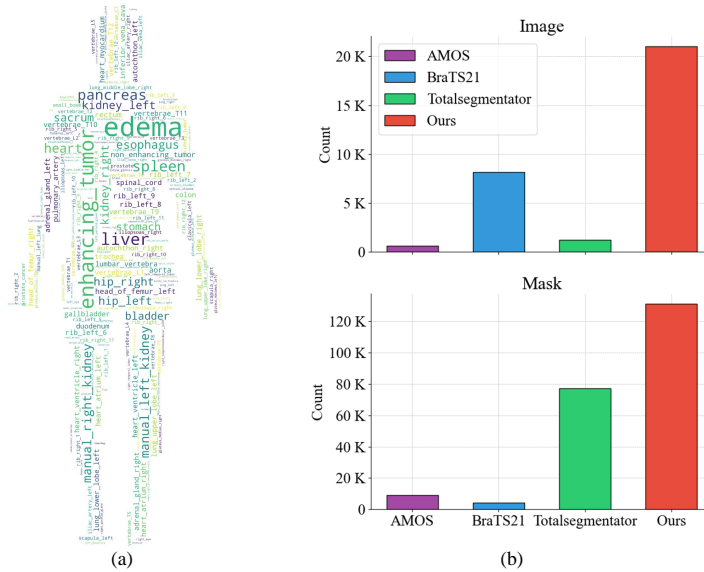


Figure 2: (a) The word cloud maps for all training data category statistics. There are 247 categories in our training data. (b) Comparison of counts of images and masks in the 3D medical image datasets we collected for training. Our dataset consists of 21K 3D images with corresponding 131K 3D masks, while *AMOS* [19], *TotalSegmentator* [44] have less than 2K images, and *BraTS21* [1] has less than 10K masks.

In addition, we conducted an extensive evaluation to examine the performance of SAM-Med3D, detailed in Section 5.2. Initially, we conducted assessments on SAM, SAM-Med2D, and our SAM-Med3D utilizing 15 public datasets. Subsequently, we delved into a thorough analysis of the results from the perspective of anatomical structures, modalities, and categories to evaluate their performance for general volumetric medical image segmentation. Besides, we also tested the transferability of the SAM-Med3D encoder on multiple fully-supervised segmentation tasks. These assessments underscore the advantages of SAM-Med3D from two perspectives: **(1) Better efficiency:** SAM-Med3D demonstrates competitive performance in comparison with 2D fine-tuned SAM but requires fewer prompt points. This ensures that, compared to previous 2D methods, physicians and professionals can utilize SAM-Med3D more readily and enjoy significantly faster speeds than per-slice interaction. **(2) Extensive segmentation capabilities:** Compared to previous works, SAM-Med3D exhibits broad segmentation capabilities across a wide array of targets and image modalities. This versatility underscores SAM-Med3D’s potential applicability in a multitude of clinical settings, showcasing its adaptability and effectiveness in addressing diverse medical imaging challenges.

2 Related Works

2.1 Vision Foundation Model

Drawing from the powerful language foundation models (LFM) like GPT-4, recent researches have seen the birth of Vision Foundation Models (VFM) [43, 21, 33, 34, 49, 10, 20]. Renowned for their zero-shot and few-shot generalization, these VFMs show outstanding adaptability to tasks or domains via established pre-training and tailored fine-tuning methods. For instance, CLIP [33] provides a pair of vision and language model pre-trained on large-scale language-image pairs, which presents excellent zero-shot generalization ability for various tasks including classification, video understanding, and image manipulation. DALL·E 2 [35] is trained based on large-scale transformer architecture, and exhibits outstanding text-to-image generation ability. SegGPT [43] converts various segmentation data into a standardized image format and pioneers a unified approach to varied segmentation tasks. SEEM [49] offers an all-in-one method using varied prompts to segment and identify items in images or videos at once. SAM [21], equipped with pre-training on a staggering 1 billion masks, has emerged as a versatile VFM for promptable image segmentation, exhibiting impressive zero-shot performance in diverse visual tasks. Due to its strong generalizability, SAM, combined with other methods, has been applied in numerous applications, including Captioning, Data Annotation, Inpainting, and Tracking [46]. However, it still shows limitations in Medical Imaging, Camouflage, and Shadow [4]. Besides, it should be emphasized that these VFMs have not been specifically tailored for medical image analysis.

2.2 SAM for Volumetric Medical Images

The success of SAM [21] in natural images has led researchers to explore its applicability in the medical imaging domain. Presently, a majority of the efforts have been concentrated on fine-tuning SAM on medical imaging data or employing SAM as a component of the whole pipeline for medical image analysis. Given that SAM is inherently a segmentation model, our emphasis lies in its application to 3D medical image segmentation, a predominant challenge in medical image analysis. MedLSAM [23] adopts SAM in a two-stage model with a localization model to furnish precise prompt, thereby enhancing SAM’s segmentation accuracy. SAM3D [2] leverages the native SAM encoder as its image Encoder. This model processes voxel images slice-by-slice to procure 3D representations, which are subsequently interpreted through a 3D Decoder to generate masks. SAM^{Med} [38] innovatively proposes a pipeline centered on generating 3D prompts from 2D points. Besides, other methods try to design 3D adapters to fine-tune SAM. 3DSAM-Adapter [11] and MA-SAM [3] have fashioned 3D adapters tailored for each SAM component, transforming the original SAM structure with 3D convolution to facilitate 3D prompt recognition and 3D mask formation. In contrast, MSA [45] retains all the weights of the original SAM and introduces space and depth adapters specifically designed to process 3D spatial information. Nonetheless, these methods encode the vital 3D information based on adapters (only partial parameters are trainable) and only fine-tune SAM on specific limited-scale medical datasets.

2.3 Evaluation of SAM in Medical Imaging

Several studies have delved into evaluating the capabilities of SAM for medical image segmentation. Cheng et al. [5] conducted a thorough assessment on 12 open-source medical image datasets, considering promptless models, models using varying numbers of point prompts, as well as models with box prompts subjected to 5 different jitter levels. Their findings suggest that SAM’s performance is typically below that of the state-of-the-art methodologies. Building on this theme, Huang et al. [16] evaluated SAM’s zero-shot capability across 52 public datasets utilizing three distinct prompts. They also observed a subpar performance of SAM on a variety of medical image segmentation tasks. Deng et al. [8] delved into SAM’s ability to segment tumors and tissues under varied prompt scenarios. Their results revealed SAM’s proficiency to be more pronounced for segmenting larger connected entities. Contrarily, Zhou et al. [48] assessed SAM’s aptitude in colonoscopy polyp segmentation without prompts, identifying a tangible potential for enhancement when using SAM for polyp segmentation. Adding another dimension to this, Hu et al. [15] centered their analysis on SAM’s performance in multi-phase liver tumor segmentation in CT scans, with a specific focus on the role of point prompts. Their results indicated that SAM’s efficacy increased with the number of point prompts. Understanding SAM’s effectiveness on expansive medical image datasets is of paramount importance.

Such insights can help the community understand what affects the model’s ability to recognize medical objects and provide ideas to improve basic medical segmentation methods. As a natural continuation of these inquiries, our research offers an extensive evaluation on volumetric medical images for several SAM methods, including our SAM-Med3D.

3 Large-Scale Volumetric Medical Dataset

3.1 Data Acquisition

3.1.1 Training

We constructed a volumetric medical image segmentation dataset for training based on numerous public and private 3D medical image datasets. The dataset contains 21K medical images and 131K masks which is probably the largest volumetric medical image segmentation dataset to date. The dataset covers 27 modalities (CT and 26 MRI sequences) and 7 anatomical structures. As shown in Figure 2, there are over 240 categories of targets including both organs and lesions. It is about 20 times larger than the largest well-known medical image segmentation dataset for organ, *TotalSegmentator* [44].

This massive dataset provides a rich resource for research and development in the field of medical image segmentation. It will allow researchers to train more complex and accurate models that will help doctors better understand and analyze medical images, and further provide more accurate information for diagnosis and treatment. In addition, the diversity of covering multiple imaging modalities and anatomical structures makes this dataset have a wide range of potential applications in different fields of medical research and clinical practice.

3.1.2 Evaluation

In the evaluation phase, we selected 13 public benchmark datasets to scrutinize various clinical scenarios, and incorporated 2 additional datasets from the MICCAI 2023 Challenge to validate the performance of different models. This validation set encompasses seven crucial anatomical structures, such as thorax and abdominal organs, brain structures, bones, and more. It also includes five types of lesions that hold significant interest in the medical field, and a range of volumetric modalities, including CT, US (Ultrasound), and eight MRI sequences. Furthermore, it contains challenging, previously unseen targets, culminating in a total of 153 distinct targets across various categories. Our validation set is three-fold:

Organ segmentation benchmark includes *Totalseg-Test* (official test set of *Totalsegmentator* [44]), *AMOS-Val* (official validation set of *AMOS* [19]), *BTCV* [22] and *HaN-Seg* [31]. In addition to the datasets with official splits, we utilized all the labeled data from *HaN-Seg* and *BTCV* for testing. These four datasets jointly offer masks for more than 100 kinds of organs across different anatomical structures throughout the body, covering both CT and MRI modalities. Notably, *HaN-Seg* offers annotations for organs-at-risk, presenting a greater challenge in our validation set than typical benchmarks.

Brain structure segmentation benchmark contains *FeTA21* [30], *FeTA22* [30], *iSeg17* [41], *iSeg19* [36], *MRBrains13* [29], *MRBrains18* [7], and *cSeg22* [37]. These seven datasets collectively provide annotations of various brain structures in multiple MRI sequences, including the brain, brainstem, and cerebellum. All the labeled data from these datasets are utilized for testing. Furthermore, *Totalseg-Test* and *HaN-Seg* provide masks for brain structures in CT images. These datasets together constitute a challenging benchmark due to their varied data sources and intricate differences in MRI sequences.

Lesion segmentation benchmark consists of *KiTS21-Val* (official validation set of *KiTS21* [14]), *BraTS21-Val** (our validation set of *BraTS21* [1]), *ATLAS* [32] and *TDSC-ABUS* [40]. For brain tumor evaluation, we randomly selected 90 cases from *BraTS21* [1] to construct *BraTS21-Val**, maintaining consistent data scale with *KiTS21-Val*. Regarding the additional dataset from MICCAI2023 Challenge (i.e. *ATLAS* and *TDSC-ABUS*), all of their labeled data are used for evaluation. It is paramount to note that these two datasets offer annotations for tumor types not encountered during training (i.e. unseen targets), with *TDSC-ABUS* introducing an unseen modality: US (Ultrasound). Both *ATLAS* and *TDSC-ABUS* are instrumental in gauging the method’s generalization capabilities.

3.2 Data Processing

To standardize these diverse data, we clean and process all the collected data in the following four steps:

1) Data cleaning based on meta information. We first summarize the meta information of the collected data, including the depth, width, and height of each medical image. We removed all cases with a physical size below 1 cm^3 or with any single dimension shorter than 1.5 cm to enable the visibility of target masks.

2) Mask cleaning based on connected domains. In the process of calculating the connected domain, we first split the original multi-class masks into multiple one-hot formats for multiple categories. Then we calculate the size of the top-5 largest connected domains and the background for each one-hot mask. With the summarized information of these masks, we remove those masks whose background occupies more than 99% of the whole volume.

3) Label quality improvement based on connected domains. As for the filtered masks, we designed a connected-domain-based pipeline to improve the label quality. Based on the summarized information of the top-5 largest connected domains for each mask, we simply remove any other domains smaller than these 5 connected domains to reduce noise.

4) Label quality improvement based on symmetry. Finally, we split the masks of some symmetric targets into paired masks of different categories. For instance, we split masks of *Kidney* into *Left Kidney* and *Right Kidney*. This step is designed to enhance the semantic consistency across different categories of masks, aiming to prevent the model from being confused about whether to segment the entire structure or just the individual left and right parts. To address this issue, SAM generates multiple predictions for each prompt and employs an additional head to generate scores, facilitating the selection of the most appropriate prediction. Given that masks of medical images typically exhibit less ambiguity, we opt to directly manipulate the data to eliminate such ambiguity, thereby enhancing the semantic consistency across mask categories and reducing the network training complexity.

4 Method

4.1 Revisit SAM

The Segment Anything Model (SAM) presents a robust architectural design for promptable image segmentation tasks, primarily tailored for 2D natural images. SAM’s architecture can be divided into three core components:

Image encoder SAM leverages an MAE [13] pre-trained Vision Transformer (ViT) [9] to extract representations. This component utilizes 2D patch embeddings combined with learnable position encodings to turn the input image into image embeddings.

Prompt encoder This module can handle both sparse (points, boxes) and dense (masks) prompts. Sparse prompts are represented using frozen 2D absolute positional encodings and then combined with learned embeddings specific to each prompt type. Dense prompts are encoded with a 2D convolution neck to generate dense prompt embeddings.

Mask decoder A lightweight structure is adopted to efficiently map the image embedding with a set of prompt embeddings to an output mask. Four steps are contained in each transformer layer: (1) self-attention on tokens; (2) cross-attention between tokens and the image embedding; (3) token updates using a point-wise MLP; (4) cross-attention that updates the image embedding with prompt details. After processing through the transformer layers, the feature map undergoes up-sampling and is subsequently converted into segmentation masks using an MLP. Notably, all the transformer layers capture only 2D geometric information during the forward pass.

4.2 Modify SAM for Volumetric Medical Images

While SAM excels in prompt-based segmentation on 2D natural images, the 2D architecture of SAM fails to capture 3D spatial information of volumetric images, leading to sub-optimal performance. We aim to modify the 2D components of SAM to fit the volumetric medical images, which leads to a new model named SAM-Med3D. The SAM-Med3D utilizes a holistic 3D structure to capture

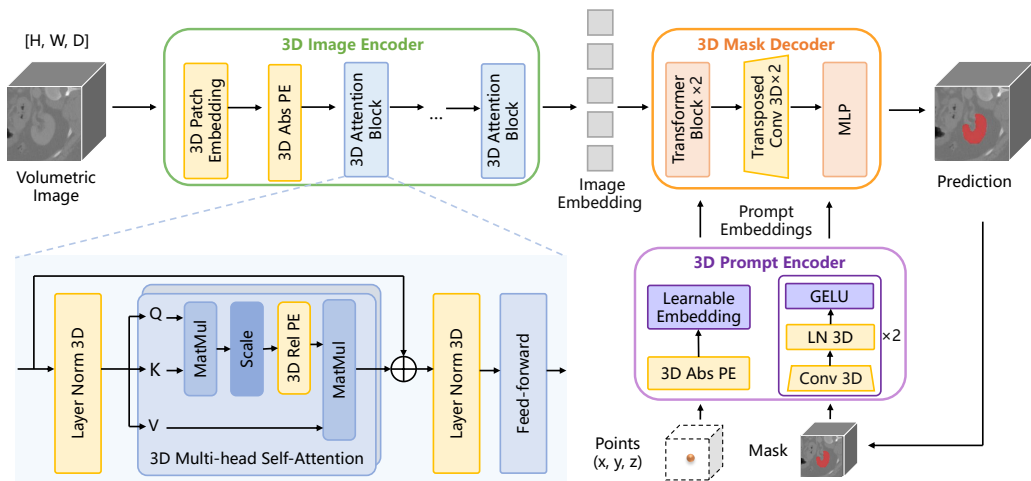


Figure 3: The modified 3D architecture of our SAM-Med3D. The original 2D components are transformed into their 3D counterparts, encompassing a 3D image encoder, 3D prompt encoder, and 3D mask decoder. 3D convolution, 3D positional encoding (PE) and 3D layer norm are employed to construct the 3D model.

spatial information directly. In the 3D Image Encoder, patches are firstly embedded using a 3D convolution with a kernel size of (16, 16, 16) and paired with a learnable 3D absolute Positional Encoding (PE). This encoding is obtained by naturally extending an additional dimension to SAM’s 2D PE. The embeddings of patches are then input to 3D attention blocks. For the 3D attention block, we incorporate a 3D relative PE into the Multi-Head Self-Attention (MHSA) module of SAM, enabling it to directly capture spatial details. Within the prompt encoder, sparse prompts leverage the 3D position encodings to represent 3D spatial nuances, while dense prompts are handled with 3D convolutions. Likewise, the 3D Mask Decoder is integrated with 3D upscaling procedures, employing 3D transposed convolution.

Due to the significant domain gap between 2D natural images and 3D medical images, we have devised a preliminary experiment to compare the impact of pre-trained weights of SAM on our SAM-Med3D. The straightforward solution to reusing SAM’s weights for a 3D model is to adopt a weight-copying strategy for these layers in which the weights’ shape exhibits differences. Taking convolution as an example, we duplicated the kernel of the 2D convolution D times and stacked them to formulate 3D convolution, where D represents the size of the kernel in the third dimension. Adopting this strategy, we trained SAM-Med3D on the AMOS dataset for 250K iterations, with and without pre-trained weights, and conducted tests on two common categories, spleen and liver.

Target	Dice with 10 points	
	w/o SAM pre-train	w/ SAM pre-train
Spleen	80.31	76.53
Liver	88.23	86.61
Average	84.27	81.57

Table 2: Preliminary experiment investigating the reusability of 2D SAM pre-trained Weights in SAM-Med3D. Experimental details are consistent with Section 5.1.

From Table 2, it can be seen that using SAM pre-trained weights did not bring a significant improvement to our SAM-Med3D. Thus, we chose an aggressive strategy, training our 3D model from scratch with large-scale volumetric medical data described in Section 3.

4.3 Evaluate SAM-Based Models on Volumetric Medical Images

Evaluation of performance is vital for understanding the capacities of algorithms and deepening researchers’ knowledge of these algorithms. Detailed and accurate evaluations help the research community grasp an AI model’s core abilities, which in turn can lead to improved effectiveness and wider applicability. In the realm of medical imaging, most evaluations of SAM-related models mainly address 2D medical images, like X-rays or endoscopic images. However, there is an evident gap in the evaluation of 3D segmentation tasks. Given that 3D segmentation plays a crucial role in medical image analysis, we undertake a thorough evaluation of SAM, SAM-Med2D (the state-of-the-art finetuned SAM for medical images), and our proposed SAM-Med3D, aiming to set a benchmark for promptable segmentation tasks on 3D medical images.

In terms of data, as mentioned in Section 3, we have constructed a representative validation set for 3D volumetric segmentation based on 13 different public datasets. This dataset encompasses a variety of targets and modalities. This evaluation will assist us in investigating the performance of SAM-Med3D in 3D volumetric segmentation tasks from multiple dimensions, including modality, anatomical structure, organs, and lesions.

We also evaluate the efficiency of models. The major concern on the efficiency is to reduce the manual work, which mainly comes from the manually-provided prompts. In terms of the prompt, we simulated a clinical scenario of interactive segmentation with point prompt mode for all models. For both 2D slice and 3D volume, we randomly sampled a point from the foreground as the first prompt, and the following points were randomly selected from the error region. It is worth noting that while 2D SAM methods (SAM, SAM-Med2D) infer on a slice-by-slice basis, our SAM-Med3D operates using a patch-based inference approach. This is in line with state-of-the-art medical image segmentation methods such as nnUNet [18], conferring an advantage to SAM-Med3D in terms of inference time. Besides, the 2D method conducts independent interactions on each slice when inferring the 3D medical image, while the 3D method only conducts global interactions on volume. This means that the number of interactions performed by 2D is actually N times that of 3D (N represents the number of slices containing objects, which typically ranges from 10 to 200). Even though 2D methods employ much more prompt points, their inherent lack of inter-slice interaction imposes a clear performance ceiling, especially on relatively complex 3D structures.

5 Experiments

5.1 Implementation details

Our method is implemented in PyTorch and trained on 8 NVIDIA Tesla A100 GPUs, each with 80GB memory. We use the Adam optimizer with an initial learning rate of $8e-4$ and train for a total of 800 epochs. During each 200-epoch cycle, the learning rate was reduced to a tenth of its original value at the 120th, 160th, and 190th epochs. Subsequently, the learning rate was restored to its initial value at the completion of each 200-epoch cycle. This procedure was iterated for a total of four loops. During training, our patch-based pipeline will crop or pad all images to a resolution of $128 \times 128 \times 128$. This crop-or-pad strategy involves padding the edges with zeros for images with width, height, and depth smaller than 128 while using trilinear interpolation to resize images in other cases. The loss function supervising the mask predictions is a DiceCELoss (Averaged Dice loss and CE loss). During our parallel training, the in-total batch size was set to 12, and the interval for aggregation and update of gradient accumulation strategy was set to every 20 steps, with a weight decay of 0.1. As for the data augmentation, we use RandomFlip and perform ZNormalization on each medical image data.

5.2 Quantitative Evaluation

5.2.1 Overall Performance

Table 3 presents the performance metrics of SAM, SAM-Med2D, and our proposed SAM-Med3D on the validation set. Our experiments reveal that SAM-Med2D, which is SAM fine-tuned with medical domain knowledge, clearly outperforms SAM. Notably, with just a single prompt point per slice, SAM’s Dice score is 25.74% less than SAM-Med2D. In contrast, our SAM-Med3D shows an even more pronounced performance leap, registering a Dice score improvement of 32.90%, or 49.91% in absolute terms. Crucially, SAM-Med3D consistently exceeds both SAM and SAM-Med2D across

Model	Prompt	Resolution	T_{inf} (s)	Overall Dice
SAM	N points	$1024 \times 1024 \times N$	13	17.01
SAM-Med2D	N points	$256 \times 256 \times N$	4	42.75
SAM-Med3D	1 point	$128 \times 128 \times 128$	2	49.91
SAM	$3N$ points	$1024 \times 1024 \times N$	19	31.86
SAM-Med2D	$3N$ points	$256 \times 256 \times N$	7	54.61
SAM-Med3D	3 points	$128 \times 128 \times 128$	3	56.38
SAM	$5N$ points	$1024 \times 1024 \times N$	25	44.72
SAM-Med2D	$5N$ points	$256 \times 256 \times N$	10	55.10
SAM-Med3D	5 points	$128 \times 128 \times 128$	4	58.57
SAM-Med3D	10 points	$128 \times 128 \times 128$	6	60.94

Table 3: Quantitative comparison of different methods on our evaluation dataset, detailed in Section 3. Here, N denotes the count of slices containing the target object ($10 \leq N \leq 200$). T_{inf} (Inference time) is calculated with $N=100$, excluding the time for image processing and simulated prompt generation.

varied prompt point counts, even though it is provided fewer points than the 2D models. Another significant advantage of our SAM-Med3D is its computational efficiency: owing to the holistic 3D architecture and lower resolution per slice, it takes just 15% of SAM’s inference time, while still delivering superior Dice scores across different numbers of points.

5.2.2 Evaluation on Different Anatomical Structures

Model	Prompt	Anatomical Structure						Lesion	
		A&T	Bone	Brain	Cardiac	Gland	Muscle	Seen	Unseen
SAM	N points	17.19	22.32	17.68	2.82	11.62	3.50	12.03	8.88
SAM-Med2D	N points	46.79	47.52	19.24	32.23	43.55	35.57	26.08	44.87
SAM-Med3D	1 point	46.80	54.77	34.48	46.51	57.28	53.28	42.02	40.53
SAM	$3N$ points	28.81	47.60	35.63	4.84	20.53	7.32	25.42	14.21
SAM-Med2D	$3N$ points	53.65	63.36	37.71	34.77	49.64	52.84	43.79	46.87
SAM-Med3D	3 points	52.01	63.64	37.82	49.51	60.94	61.10	47.36	44.92
SAM	$5N$ points	39.57	65.87	37.68	8.03	33.25	15.06	39.95	23.22
SAM-Med2D	$5N$ points	54.14	63.78	38.81	34.83	49.92	53.24	45.15	47.66
SAM-Med3D	5 points	53.60	66.54	39.08	51.37	62.66	64.22	48.75	45.71
SAM-Med3D	10 points	55.81	69.13	40.71	52.86	65.01	67.28	50.52	48.44

Table 4: Comparison from the perspective of anatomical structure and lesion. A&T represents Abdominal and Thorax targets. N denotes the count of slices containing the target object ($10 \leq N \leq 200$).

In order to gain insight into the performance of SAM-Med3D, we divided the evaluation results on our validation set according to the anatomical structures. Our validation set covers a wide range of anatomical structures including various kinds of organs (abdominal, thorax, cardiac, bone, gland, and muscle), brain structures, and five types of lesions. Table 4 summarizes the evaluation results of SAM, SAM-Med2D, and our SAM-Med3D. When only provided with N points (1 point/slice), SAM often segments the wrong target, and this tendency is difficult to correct even when multiple points are provided (especially on the anatomical structures without clear boundaries, such as cardiac and muscle). However, with the incorporation of medical knowledge, SAM-Med2D and our SAM-Med3D are more likely to locate the correct target even with just one point on each slice/volume. Given only one point (N times fewer than 2D methods), our SAM-Med3D demonstrates competitive performance with SAM-Med2D across all anatomical structures, with a maximum boost of 17.71% in the Dice score.

As the number of prompt points increases, our SAM-Med3D maintains a leading position in the segmentation of most anatomical structures. Notably, abdominal and thorax targets do not follow this leading trend, wherein 2D and 3D approaches exhibit comparable performance. This exception can be ascribed to the simpler 3D structure of these targets, which diminishes the reliance on 3D spatial details. Analogous observations can be made for structures like bones where SAM surpasses

SAM-Med2D when given $5N$ points. We attribute this to the relatively clear boundaries of the bone, which lowers the difficulty of segmentation and allows SAM to accurately locate bone objects as long as sufficient prompt information is provided.

In our evaluation, we considered both seen and unseen lesions across various methods. Table 4 illustrates that our SAM-Med3D consistently outperforms other methods for seen lesions. Regarding the generalization to unseen lesions, SAM-Med3D exhibits sub-optimal performance when provided with limited prompts, and this limitation is mitigated with an increased number of prompts. Notably, SAM-Med3D achieves a performance of 48.44% with 10 prompts, in comparison to SAM-Med2D’s 47.66% using N prompts where $10 \leq N \leq 200$.

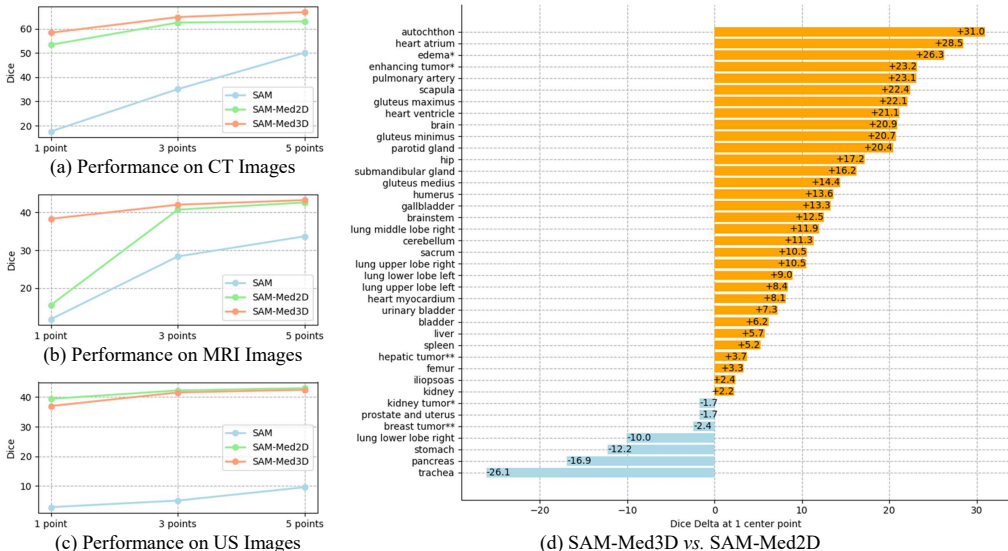


Figure 4: (a-c) Performance comparison across different modalities with varying numbers of points. Notably, while SAM-Med2D was trained on the US (Ultrasound) modality and SAM-Med3D was not, SAM-Med3D still exhibits competitive performance. (d) Comparison of the Dice coefficient between SAM-Med3D and the top-performing 2D fine-tuned SAM model, SAM-Med2D [6] across 34 major organs and 5 kinds of lesions. * and ** represent seen and unseen lesions.

5.2.3 Evaluation on Different Modalities

We compared the three methods for three dominant modalities in volumetric medical imaging (CT, MRI, and US) across various numbers of prompt points. Regarding to multi-modal data, we validated all methods for each single modality. For brevity, we averaged the results from all MRI sequences to present them more effectively as MRI modality results.

From our evaluations, SAM struggles to segment across all three volumetric modalities with just a single point per slice, resulting in Dice scores below 20%. With the provision of five prompt points per slice, SAM starts exhibiting initial credible segmentation outcomes for CT. Nonetheless, for MRI and US, an increased number of points (> 5 pt/slice) remains essential for SAM to effectively locate and segment the medical targets. Moreover, the incorporation of medical knowledge can significantly help SAM to discern medical targets in all three modalities. As shown in Figure 4 (a, c), when provided with a single point per slice/volume, SAM-Med2D and SAM-Med3D outperform SAM with a clear margin on CT and US images. It is worth noting that SAM-Med3D gets competitive performance with SAM-Med2D with N times fewer prompt points (N denotes the count of slices containing the target object).

Furthermore, we notice in Figure 4 (b) that when provided a single prompt point, the performance of 2D SAM methods on MRI images was markedly inferior to that of our proposed SAM-Med3D. Regardless of the inclusion of medical knowledge during the training phase, both SAM and SAM-Med2D show this disadvantage, which was never observed in 2D evaluation [6]. We think this discrepancy arises from the complexity associated with image processing for 3D and 2D MRI images.

MRI encompasses diverse types of sequences and phases (e.g. T1, T2, FLAIR), resulting in various intensity ranges (varying from [0,1024] to [0,65535]) and significantly different patterns of images. Notably, during the 2D training process, images are stored in standard 2D image formats like PNG or JPEG, which possess an intensity range confined between 0 and 255. To employ 3D MRI data for 2D training, we need to clip and normalize the original value into a limited range. This limitation engenders a loss in detail of the MRI images. Consequently, even after the adaptation to medical images, the first-click performance of 2D SAM methods on MRI images remains sub-optimal when compared to 3D methods that holistically work on the 3D images.

5.2.4 Evaluation on Major Organs and Lesions

Figure 4 (d) presents the comparison between our SAM-Med3D using 1 point and SAM-Med2D using N points per volume. SAM-Med3D gains higher results for 39 targets (34 organs and 5 lesions), with a maximum delta value of +31.0%. Consistent with the observation in Section 5.2.2, SAM-Med3D shows a greater boost for muscle, gland, and cardiac targets such as autochthon, parotid gland, and heart atrium, and shows minor improvement for some abdominal organs (e.g. +2.2% for kidney, +5.2% for spleen). We hypothesize that the fundamental cause of this disparity may be attributed to varying sensitivities to inter-slice information. For instance, certain abdominal organ categories, such as the kidney and stomach, possess a relatively large scale across the majority of slices in which they are present. Thus, 2D methods are already sufficient to segment them into individual slices. In contrast, categories like the autochthon and pulmonary artery, while occupying smaller volumes on a single slice, have heightened demand for continuity across slices. Consequently, they are more effectively segmented by SAM-Med3D, which takes inter-slice information into account.

As for lesions, SAM-Med3D exhibited an improvement of over 20% in both edema and enhancing tumor. However, its performance on kidney tumors was even inferior to that of SAM-Med2D. This can be attributed to the same causes (i.e., different sensitivity to inter-slice information). Compared with kidney tumors, both edema and enhancing tumors exhibit more complex 3D spatial structures, emphasizing the significance of capturing inter-slice contextual details. Regarding unseen lesions, SAM-Med3D shows around 4% improvement for hepatic tumors and shows minor degradation in breast tumors. The root cause can be the common modality used to detect breast tumors is US (Ultrasound), which is unseen in our training.

5.2.5 Evaluation on Transferability

Dataset	UNETR	
	w/o pre-train	w/ pre-train
AMOS [19]	76.29	81.92
Totalsegmentator [44]	82.67	85.17
Average	79.48	83.55

Table 5: Transferability evaluation for the fully-supervised 3D medical image segmentation. We trained the state-of-the-art ViT-based segmentation model (i.e. UNETR [12]), both with and without our SAM-Med3D pre-trained ViT encoder, to assess the benefits of pre-training.

We also conduct a test of transferability on two frequently-used benchmarks for 3D medical image segmentation based on UNETR [12], the leading-edge ViT-based model in this task. As depicted in Table 5, when fine-tuned with the pre-trained ViT encoder from our SAM-Med3D, UNETR demonstrates a substantial performance boost compared to configurations without pre-training, achieving a maximum improvement of 5.63% in the Dice score. Consequently, our SAM-Med3D not only demonstrates the substantial potential to establish itself as a foundational model for 3D medical image analysis but also facilitates the community in exploring the viability of diminishing inductive bias during pre-training within the medical image realm. To the best of our knowledge, SAM-Med3D may be positioned as the first ViT-based foundational model for 3D medical images.

5.3 Visualization

To qualitatively compare the segmentation masks of SAM-Med3D and other methods, we visualize the results across varying numbers of points. To maintain the fairness of comparison, we uniformly

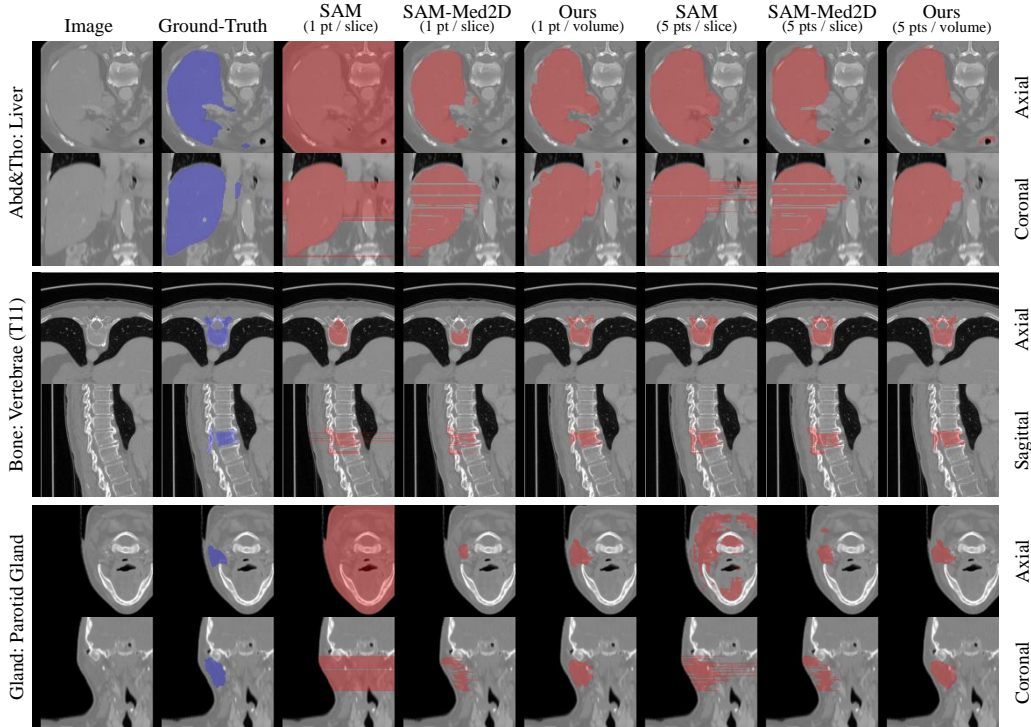


Figure 5: Visualization of SAM, SAM-Med2D, and our proposed SAM-Med3D across diverse anatomical structures for varying numbers of point. We present both axial slices and coronal/sagittal views to comprehensively illustrate the 3D results. Abd&Tho denotes Abdominal and Thorax.

resample the 3D images into the spacing of 1.5 mm in each axis and test them with the best resolution of each method (1024^2 for SAM, 256^2 for SAM-Med2D and 128^3 for SAM-Med3D). These settings of evaluation (i.e. resolution and prompt simulation) are optimal for each method. Figure 5 illustrates the segmentation outcomes for various anatomical structures, such as Abd&Tho, Bone, and Gland. Meanwhile, Figure 6 visualizes cases from the perspective of modalities, including CT and two MRI sequences. For each visualized case, two views are depicted: (1) Axial: This horizontal cross-section divides the body or an organ into upper and lower segments. It stands as the most frequently utilized perspective for observing organ anatomy. (2) Sagittal/Coronal: Representing a vertical cross-section, this view divides the body or organ into left/right or anterior/posterior sections. Notably, in contrast to many other segmentation studies, we introduce this view to enhance the depiction of relations between each slice throughout the predicted 3D volume for each method.

Based on these visualization results, we highlight two key observations:

SAM-Med3D requires significantly fewer prompts. As shown in Figure 5, given varying points, the boundaries in the visual results from our SAM-Med3D consistently approximate the ground truth more closely than other methods. This is particularly evident in the case of the gland (the fifth and sixth rows). We believe this is because the gland has somewhat ambiguous boundaries and a relatively smooth and regular 3D structure. Figure 6 shows our SAM-Med3D consistently surpasses other methods across various modalities. These findings underscore that our SAM-Med3D offers superior usability (i.e., achieving better outcomes with significantly fewer prompt points) compared to all 2D SAM models in the context of 3D medical image segmentation tasks.

SAM-Med3D exhibits better inter-slice consistency. Further analysis reveals that our SAM-Med3D consistently achieves superior inter-slice consistency compared to all 2D SAM methods when observed from sagittal/coronal perspectives (as evident in the second, fourth, and sixth rows of Figure 5 and Figure 6). Specifically, when provided with a single prompt point, the stability of all 2D methods across various slices falters. While they can adeptly segment the target in certain slices, others result in either empty outputs or erroneously classifying the entire region as the target. Such inconsistencies manifest as discernible inter-slice discrepancies, such as gaps between slices or

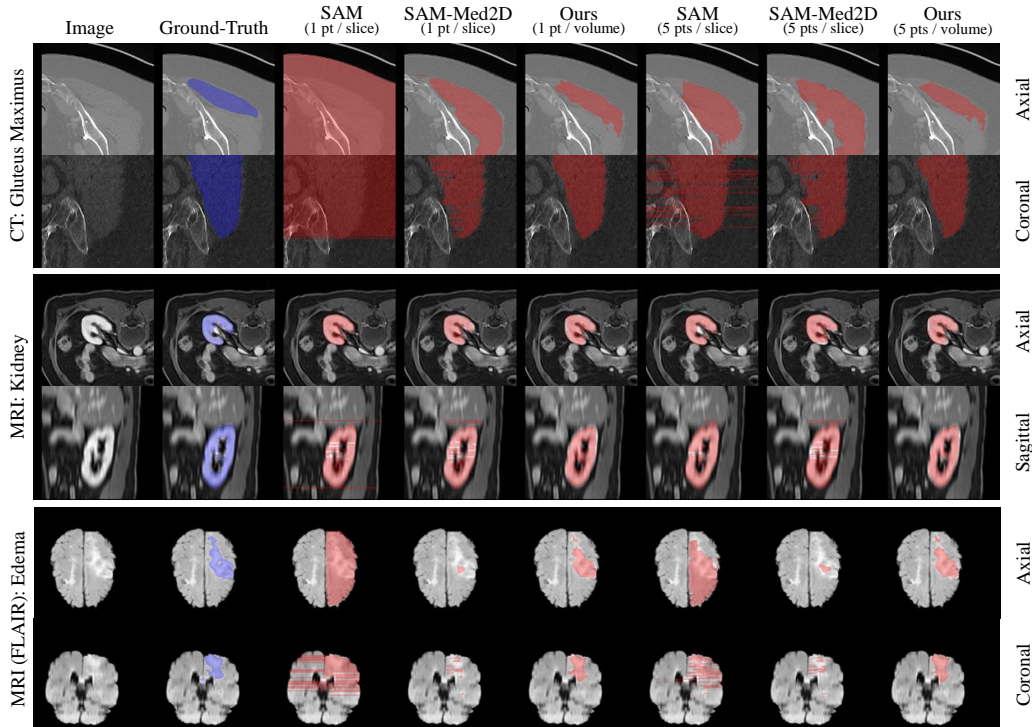


Figure 6: Visualization of SAM, SAM-Med2D, and our proposed SAM-Med3D across various modalities for varying numbers of point. We present both axial slices and coronal/sagittal views to comprehensively illustrate the 3D results.

glaring inaccuracies on specific slices, especially when observed from vertical viewpoints like sagittal and coronal views. We attribute this shortcoming to an intrinsic limitation of all 2D SAM methods: segmenting based on individual 2D slices neglects the crucial 3D spatial context of the entire volume. As the number of points provided for each slice increases, this shortcoming is somewhat mitigated. However, it also results in a burdensome increase in annotation workload. Conversely, with fewer prompt points, our SAM-Med3D method consistently produces results with enhanced consistency across slices, thanks to the integration of 3D spatial information.

6 Conclusion

In this study, we present SAM-Med3D, a holistic 3D SAM model for volumetric medical image segmentation, trained from scratch on a large-scale 3D medical image dataset. Our SAM-Med3D employs 3D positional encodings in different components to directly integrate 3D spatial information, and exhibit excellent performance on volumetric medical image segmentation. SAM-Med3D achieves a 32.90% improvement than SAM when provided with 1 point per volume, indicating its excellent usability to generate better outcomes in volumetric medical segmentation tasks with significantly fewer prompt points.

Furthermore, we conduct an extensive evaluation from diverse perspectives to explore the capacities of SAM-Med3D. For various anatomical structures like bone, heart and muscle, our SAM-Med3D outperforms other methods with a clear margin when limited prompt is provided. Our SAM-Med3D consistently excels in different modalities and various organs and lesions. Additionally, we test the transferability of SAM-Med3D. Validated on two frequently used benchmarks, SAM-Med3D has the potential to work as a powerful pre-trained model for 3D medical image transformer.

Setting aside the numerical result gap between 2D SAM methods and our SAM-Med3D, a well-trained 3D SAM model should inherently exhibit superior inter-slice consistency and usability, as observed in the visual results. While 3D models enhance usability, prompts within volumetric images

tend to be sparser compared to the densely annotated 2D slices used in slice-by-slice inference. This sparsity places significant demands on the 3D model’s ability to capture spatial information and effectively utilize sparse prompts, thereby increasing the training complexity. In our approach, we address this issue by employing a fully learnable 3D structure to better model the spatial information in 3D space. Despite this, there remains a plethora of avenues for future exploration, such as the development of novel 3D prompt forms and training strategies that are more suited to 3D contexts.

References

- [1] U. Baid, S. Ghodasara, M. Bilello, S. Mohan, E. Calabrese, E. Colak, K. Farahani, J. Kalpathy-Cramer, F. C. Kitamura, S. Pati, L. M. Prevedello, J. D. Rudie, C. Sako, R. T. Shinohara, T. Bergquist, R. Chai, J. A. Eddy, J. Elliott, W. Reade, T. Schaffter, T. Yu, J. Zheng, B. Annotators, C. Davatzikos, J. Mongan, C. Hess, S. Cha, J. E. Villanueva-Meyer, J. B. Freymann, J. S. Kirby, B. Wiestler, P. Crivellaro, R. R. Colen, A. Kotrotsou, D. S. Marcus, M. Milchenko, A. Nazeri, H. M. Fathallah-Shaykh, R. Wiest, A. Jakab, M. Weber, A. Mahajan, B. H. Menze, A. E. Flanders, and S. Bakas. The RSNA-ASNR-MICCAI brats 2021 benchmark on brain tumor segmentation and radiogenomic classification. *CoRR*, abs/2107.02314, 2021. URL <https://arxiv.org/abs/2107.02314>.
- [2] N.-T. Bui, D.-H. Hoang, M.-T. Tran, and N. Le. Sam3d: Segment anything model in volumetric medical images. *arXiv preprint arXiv:2309.03493*, 2023.
- [3] C. Chen, J. Miao, D. Wu, Z. Yan, S. Kim, J. Hu, A. Zhong, Z. Liu, L. Sun, X. Li, et al. Ma-sam: Modality-agnostic sam adaptation for 3d medical image segmentation. *arXiv preprint arXiv:2309.08842*, 2023.
- [4] T. Chen, L. Zhu, C. Ding, R. Cao, S. Zhang, Y. Wang, Z. Li, L. Sun, P. Mao, and Y. Zang. Sam fails to segment anything?—sam-adapter: Adapting sam in underperformed scenes: Camouflage, shadow, and more. *arXiv preprint arXiv:2304.09148*, 2023.
- [5] D. Cheng, Z. Qin, Z. Jiang, S. Zhang, Q. Lao, and K. Li. Sam on medical images: A comprehensive study on three prompt modes. 2023.
- [6] J. Cheng, J. Ye, Z. Deng, J. Chen, T. Li, H. Wang, Y. Su, Z. Huang, J. Chen, L. Jiang, et al. Sam-med2d. *arXiv preprint arXiv:2308.16184*, 2023.
- [7] A. Crimi, S. Bakas, H. Kuijf, B. Menze, and M. Reyes. *Brainlesion: Glioma, Multiple Sclerosis, Stroke and Traumatic Brain Injuries: Third International Workshop, BrainLes 2017, Held in Conjunction with MICCAI 2017, Quebec City, QC, Canada, September 14, 2017, Revised Selected Papers*, volume 10670. Springer, 2018.
- [8] R. Deng, C. Cui, Q. Liu, T. Yao, L. W. Remedios, S. Bao, B. A. Landman, L. E. Wheless, L. A. Coburn, K. T. Wilson, Y. Wang, S. Zhao, A. B. Fogo, H. Yang, Y. Tang, and Y. Huo. Segment anything model (sam) for digital pathology: Assess zero-shot segmentation on whole slide imaging. 2023.
- [9] A. Dosovitskiy, L. Beyer, A. Kolesnikov, D. Weissenborn, X. Zhai, T. Unterthiner, M. Dehghani, M. Minderer, G. Heigold, S. Gelly, J. Uszkoreit, and N. Houlsby. An image is worth 16x16 words: Transformers for image recognition at scale. *CoRR*, abs/2010.11929, 2020. URL <https://arxiv.org/abs/2010.11929>.
- [10] A. Dosovitskiy, L. Beyer, A. Kolesnikov, D. Weissenborn, X. Zhai, T. Unterthiner, M. Dehghani, M. Minderer, G. Heigold, S. Gelly, et al. An image is worth 16x16 words: Transformers for image recognition at scale. *arXiv preprint arXiv:2010.11929*, 2020.
- [11] S. Gong, Y. Zhong, W. Ma, J. Li, Z. Wang, J. Zhang, P.-A. Heng, and Q. Dou. 3dsam-adapter: Holistic adaptation of sam from 2d to 3d for promptable medical image segmentation. *arXiv preprint arXiv:2306.13465*, 2023.
- [12] A. Hatamizadeh, Y. Tang, V. Nath, D. Yang, A. Myronenko, B. Landman, H. R. Roth, and D. Xu. Unetr: Transformers for 3d medical image segmentation. In *Proceedings of the IEEE/CVF winter conference on applications of computer vision*, pages 574–584, 2022.

- [13] K. He, X. Chen, S. Xie, Y. Li, P. Dollár, and R. Girshick. Masked autoencoders are scalable vision learners. In *Proceedings of the IEEE/CVF conference on computer vision and pattern recognition*, pages 16000–16009, 2022.
- [14] N. Heller, F. Isensee, D. Trofimova, R. Tejjpaul, Z. Zhao, H. Chen, L. Wang, A. Golts, D. Khapun, D. Shats, Y. Shoshan, F. Gilboa-Solomon, Y. George, X. Yang, J. Zhang, J. Zhang, Y. Xia, M. Wu, Z. Liu, E. Walczak, S. McSweeney, R. Vasdev, C. Hornung, R. Solaiman, J. Schoepfoerster, B. Abernathy, D. Wu, S. Abdulkadir, B. Byun, J. Spriggs, G. Struyk, A. Austin, B. Simpson, M. Hagstrom, S. Virnig, J. French, N. Venkatesh, S. Chan, K. Moore, A. Jacobsen, S. Austin, M. Austin, S. Regmi, N. Papanikolopoulos, and C. Weight. The kits21 challenge: Automatic segmentation of kidneys, renal tumors, and renal cysts in corticomedullary-phase ct, 2023.
- [15] C. Hu, T. Xia, S. Ju, and X. Li. When sam meets medical images: An investigation of segment anything model (sam) on multi-phase liver tumor segmentation. 2023.
- [16] Y. Huang, X. Yang, L. Liu, H. Zhou, A. Chang, X. Zhou, R. Chen, J. Yu, J. Chen, C. Chen, H. Chi, X. Hu, D.-P. Fan, F. Dong, and D. Ni. Segment anything model for medical images? 2023.
- [17] Z. Huang, H. Wang, Z. Deng, J. Ye, Y. Su, H. Sun, J. He, Y. Gu, L. Gu, S. Zhang, et al. Stunet: Scalable and transferable medical image segmentation models empowered by large-scale supervised pre-training. *arXiv preprint arXiv:2304.06716*, 2023.
- [18] F. Isensee, P. F. Jaeger, S. A. Kohl, J. Petersen, and K. H. Maier-Hein. nnu-net: a self-configuring method for deep learning-based biomedical image segmentation. *Nature methods*, 18(2):203–211, 2021.
- [19] Y. Ji, H. Bai, J. Yang, C. Ge, Y. Zhu, R. Zhang, Z. Li, L. Zhang, W. Ma, X. Wan, et al. Amos: A large-scale abdominal multi-organ benchmark for versatile medical image segmentation. *arXiv preprint arXiv:2206.08023*, 2022.
- [20] C. Jia, Y. Yang, Y. Xia, Y.-T. Chen, Z. Parekh, H. Pham, Q. Le, Y.-H. Sung, Z. Li, and T. Duerig. Scaling up visual and vision-language representation learning with noisy text supervision. In *International conference on machine learning*, pages 4904–4916. PMLR, 2021.
- [21] A. Kirillov, E. Mintun, N. Ravi, H. Mao, C. Rolland, L. Gustafson, T. Xiao, S. Whitehead, A. C. Berg, W.-Y. Lo, et al. Segment anything. *arXiv preprint arXiv:2304.02643*, 2023.
- [22] B. Landman, Z. Xu, J. Igelsias, M. Styner, T. Langerak, and A. Klein. Miccai multi-atlas labeling beyond the cranial vault—workshop and challenge. In *Proc. MICCAI Multi-Atlas Labeling Beyond Cranial Vault—Workshop Challenge*, volume 5, page 12, 2015.
- [23] W. Lei, X. Wei, X. Zhang, K. Li, and S. Zhang. Medlsam: Localize and segment anything model for 3d medical images. *arXiv preprint arXiv:2306.14752*, 2023.
- [24] X. Li, H. Chen, X. Qi, Q. Dou, C.-W. Fu, and P.-A. Heng. H-denseunet: hybrid densely connected unet for liver and tumor segmentation from ct volumes. *IEEE transactions on medical imaging*, 37(12):2663–2674, 2018.
- [25] J. Liu, Y. Zhang, J.-N. Chen, J. Xiao, Y. Lu, B. A. Landman, Y. Yuan, A. Yuille, Y. Tang, and Z. Zhou. Clip-driven universal model for organ segmentation and tumor detection. *arXiv preprint arXiv:2301.00785*, 2023.
- [26] X. Luo, G. Wang, T. Song, J. Zhang, M. Aertsen, J. Deprest, S. Ourselin, T. Vercauteren, and S. Zhang. Mideepseg: Minimally interactive segmentation of unseen objects from medical images using deep learning. *Medical image analysis*, 72:102102, 2021.
- [27] J. Ma and B. Wang. Segment anything in medical images. *arXiv preprint arXiv:2304.12306*, 2023.
- [28] M. A. Mazurowski, H. Dong, H. Gu, J. Yang, N. Konz, and Y. Zhang. Segment anything model for medical image analysis: an experimental study. *Medical Image Analysis*, 89:102918, 2023.

- [29] A. M. Mendrik, K. L. Vincken, H. J. Kuijff, M. Breeuwer, W. H. Bouvy, J. De Bresser, A. Alansary, M. De Bruijne, A. Carass, A. El-Baz, et al. Mrbrains challenge: online evaluation framework for brain image segmentation in 3t mri scans. *Computational intelligence and neuroscience*, 2015:1–1, 2015.
- [30] K. Payette, P. de Dumast, H. Kebiri, I. Ezhov, J. C. Paetzold, S. Shit, A. Iqbal, R. Khan, R. Kottke, P. Grehten, et al. An automatic multi-tissue human fetal brain segmentation benchmark using the fetal tissue annotation dataset. *Scientific data*, 8(1):167, 2021.
- [31] G. Podobnik, P. Strojjan, P. Peterlin, B. Ibragimov, and T. Vrtovec. Han-seg: The head and neck organ-at-risk ct and mr segmentation dataset. *Medical physics*, 50(3):1917–1927, 2023.
- [32] F. Quinton, R. Popoff, B. Presles, S. Leclerc, F. Meriaudeau, G. Nodari, O. Lopez, J. Pellegrinelli, O. Chevallier, D. Ginhac, et al. A tumour and liver automatic segmentation (atlas) dataset on contrast-enhanced magnetic resonance imaging for hepatocellular carcinoma. *Data*, 8(5):79, 2023.
- [33] A. Radford, J. W. Kim, C. Hallacy, A. Ramesh, G. Goh, S. Agarwal, G. Sastry, A. Askell, P. Mishkin, J. Clark, G. Krueger, and I. Sutskever. Learning transferable visual models from natural language supervision, 2021.
- [34] A. Ramesh, M. Pavlov, G. Goh, S. Gray, C. Voss, A. Radford, M. Chen, and I. Sutskever. Zero-shot text-to-image generation. 2021.
- [35] A. Ramesh, P. Dhariwal, A. Nichol, C. Chu, and M. Chen. Hierarchical text-conditional image generation with clip latents. *arXiv preprint arXiv:2204.06125*, 1(2):3, 2022.
- [36] Y. Sun, K. Gao, Z. Wu, G. Li, X. Zong, Z. Lei, Y. Wei, J. Ma, X. Yang, X. Feng, et al. Multi-site infant brain segmentation algorithms: the iseg-2019 challenge. *IEEE Transactions on Medical Imaging*, 40(5):1363–1376, 2021.
- [37] Y. Sun, L. Wang, V. Jewells, K. L. Humphreys, and W. Lin. MICCAI Grand Challenge on Multi-domain Cross-time- point Infant Cerebellum MRI Segmentation 2022, Mar. 2022. URL <https://doi.org/10.5281/zenodo.6362381>.
- [38] C. Wang, D. Li, S. Wang, C. Zhang, Y. Wang, Y. Liu, and G. Yang. Sammed: A medical image annotation framework based on large vision model. *arXiv preprint arXiv:2307.05617*, 2023.
- [39] H. Wang, H. Yi, J. Liu, and L. Gu. Integrated treatment planning in percutaneous microwave ablation of lung tumors. In *2022 44th Annual International Conference of the IEEE Engineering in Medicine & Biology Society (EMBC)*, pages 4974–4977. IEEE, 2022.
- [40] K. Wang. Tumor detection, segmentation and classification challenge on automated 3d breast ultrasound (abus) 2023, 2023. <https://tdsc-abus2023.grand-challenge.org/TDSC-ABUS2023/>.
- [41] L. Wang, D. Nie, G. Li, É. Puybureau, J. Dolz, Q. Zhang, F. Wang, J. Xia, Z. Wu, J.-W. Chen, et al. Benchmark on automatic six-month-old infant brain segmentation algorithms: the iseg-2017 challenge. *IEEE transactions on medical imaging*, 38(9):2219–2230, 2019.
- [42] X. Wang, L. Jiang, L. Li, M. Xu, X. Deng, L. Dai, X. Xu, T. Li, Y. Guo, Z. Wang, and P. L. Dragotti. Joint learning of 3d lesion segmentation and classification for explainable covid-19 diagnosis. *IEEE Transactions on Medical Imaging*, 40(9):2463–2476, 2021. doi: 10.1109/TMI.2021.3079709.
- [43] X. Wang, X. Zhang, Y. Cao, W. Wang, C. Shen, and T. Huang. Seggpt: Segmenting everything in context. *arXiv preprint arXiv:2304.03284*, 2023.
- [44] J. Wasserthal, H.-C. Breit, M. T. Meyer, M. Pradella, D. Hinck, A. W. Sauter, T. Heye, D. T. Boll, J. Cyriac, S. Yang, M. Bach, and M. Segeroth. Totalsegmentator: Robust segmentation of 104 anatomic structures in ct images. *Radiology: Artificial Intelligence*, 5(5):e230024, 2023.
- [45] J. Wu, R. Fu, H. Fang, Y. Liu, Z. Wang, Y. Xu, Y. Jin, and T. Arbel. Medical sam adapter: Adapting segment anything model for medical image segmentation. *arXiv preprint arXiv:2304.12620*, 2023.

- [46] C. Zhang, S. Zheng, C. Li, Y. Qiao, T. Kang, X. Shan, C. Zhang, C. Qin, F. Rameau, S.-H. Bae, et al. A survey on segment anything model (sam): Vision foundation model meets prompt engineering. *arXiv preprint arXiv:2306.06211*, 2023.
- [47] J. Zhang, Y. Xie, Y. Xia, and C. Shen. Dodnet: Learning to segment multi-organ and tumors from multiple partially labeled datasets. In *Proceedings of the IEEE/CVF conference on computer vision and pattern recognition*, pages 1195–1204, 2021.
- [48] T. Zhou, Y. Zhang, Y. Zhou, Y. Wu, and C. Gong. Can sam segment polyps? 2023.
- [49] X. Zou, J. Yang, H. Zhang, F. Li, L. Li, J. Wang, L. Wang, J. Gao, and Y. J. Lee. Segment everything everywhere all at once. 2023.